Nuclear Instruments and Methods in Physics Research B 572 (2026) 165991

Contents lists available at ScienceDirect

Nuclear Inst. and Methods in Physics Research, B

journal homepage: www.elsevier.com/locate/nimb

Full length article

Simulation and experimental validation of atom effusion characteristics for resonance ionization laser ion source geometries

Asar A.H. Jaradat [a,b,*], Reinhard Heinke [a,b], Bruce A. Marsh [a], Dominik Studer [d,e], Kara M. Lynch [b], Kieran T. Flanagan [b], Klaus Wendt [c], Matou Stemmler [c], Sebastian Raeder [d,e], Sebastian Rothe [a], Simone Gilardoni [a], Thorben Niemeyer [c], Raphael Hasse [c]

[a] STI Group, SY Department, CERN, Geneva, Switzerland
[b] Department of Physics and Astronomy, The University of Manchester, Manchester, United Kingdom
[c] Institute of Physics, Johannes Gutenberg University Mainz, Mainz, Germany
[d] GSI Helmholtzzentrum fuer Schwerionenforschung, Darmstadt, Germany
[e] Helmholtz Institute Mainz, Mainz, Germany

ARTICLE INFO

Keywords:
Resonance ionization laser ion source
Ion source geometry
Laser spectroscopy
Radioactive ion beams
Atom beam effusion

ABSTRACT

A Monte-Carlo-type simulation model has been developed to describe the effusion of atoms from hot cavity tubes for application to high-purity laser resonance ionization ion sources. The model is validated by comparison with theoretical descriptions of low-pressure particle transfer mechanisms and experimental data obtained by probing the spatial evolution of the atom density downstream for different atom source geometries with laser ionization. The numeric studies, in agreement with the experimental validation, quantify possible efficiency improvements in the order of 30% for high-purity resonance ionization laser ion sources, and highlight the significance of closest distance between atom source and active ionization region. The developed simulation model is a stepping stone for further investigations into efficiency, experimental resolution for laser spectroscopy applications, and more sophisticated geometries.

1. Introduction

Laser resonance ionization spectroscopy directly within an ion source coupled to an isotope production target has been proven to be a highly sensitive tool for nuclear structure investigations on isotopes with low production and extraction yields at radioactive ion beam facilities such as CERN-ISOLDE [1]. While the efficiency of this technique is unrivaled, the spectral resolution is ultimately limited by Doppler broadening. At an ion source temperature of ≈2000 °C typically required for efficient operation, it results in a 1–10 GHz resolution limit. Resolving hyperfine structure splittings to precisely extract nuclear structure parameters such as electromagnetic moments typically requires a resolution below the GHz regime [2]. A new laser ion source design has been implemented at ISOLDE recently to provide in-source spectroscopy capabilities down to an experimental linewidth of 100–200 MHz [3], an order of magnitude below usual limitations. It is based on the high beam purity Laser Ion Source and Trap (LIST) [4,5]. This assembly features spatial separation of atomization in the hot cavity where potential ion beam contamination can arise from non-laser related ionization mechanisms such as surface ionization, from an undisturbed laser-atom interaction volume in a radio-frequency quadrupole (RFQ) unit directly downstream, where solely element-selective laser ionization takes place. In the so-called Perpendicularly Illuminated LIST (PI-LIST) version [6], a crossed laser/atom beam geometry reduces the effective Doppler broadening due to a more narrow transversal velocity distribution in the atomic beam effusing from the source. Following the integration of this device as the standard tool for nuclear structure high-resolution laser spectroscopy applications at the RISIKO[1] off-line mass separator facility at the Institute of Physics of Johannes Gutenberg University Mainz [7,8], it has been implemented online at the ISOLDE facility at CERN [3] for nuclear structure investigations. Whilst this technique proved appropriate in applicability in ISOL facilities in general, it remains limited especially due to significant efficiency loss [3].

This work addresses increasing the efficiency of the LIST method to promote its applicability as a standard reliable ion source, and for high

* Corresponding author at: STI Group, SY Department, CERN, Geneva, Switzerland.
E-mail address: asar.a.h.jaradat@cern.ch (A.H. Jaradat).

[1] German acronym "*R*esonanz*I*onisations*S*pektroskopie *I*n *KO*llinearer Geometrie".

https://doi.org/10.1016/j.nimb.2025.165991
Received 5 September 2025; Received in revised form 10 December 2025; Accepted 25 December 2025
Available online 8 January 2026

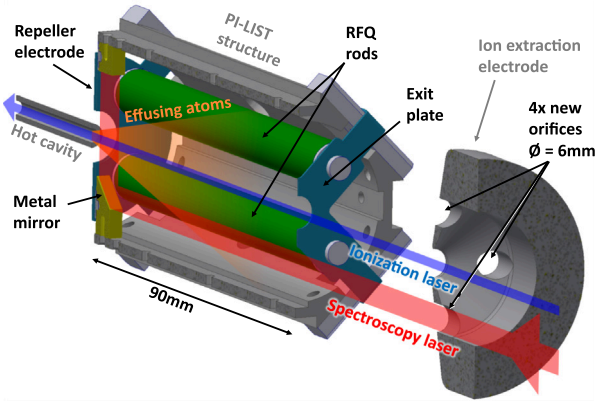

Fig. 1. 3-D half-cut representation of the PI-LIST ion source as employed at ISOLDE, including the atomizer hot cavity and adapted extraction electrode for off-axis laser beam transport.
Source: Figure taken from [3].

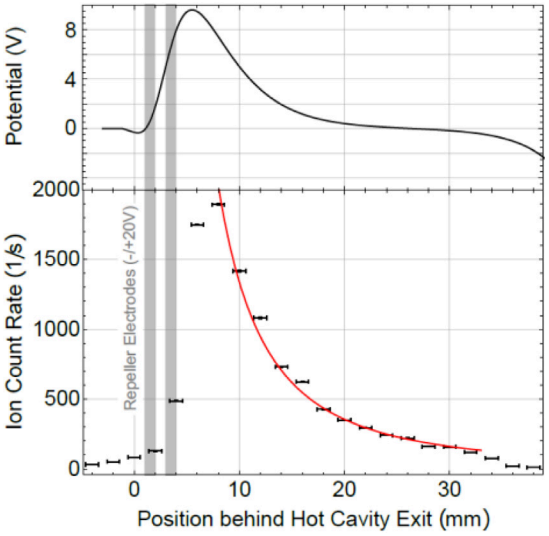

Fig. 2. Simulated electric potential (upper panel) and measured ion production rate representing atom density along the central axis (lower panel) at certain distances from the hot cavity for the Mainz PI-LIST version.
Source: Figure adapted from [10].

resolution spectroscopy methods for nuclear structure investigations at online facilities. Hereby, the focus is on the atom effusion characteristics from the hot cavity into the laser interaction volume of the LIST. In the current design, the majority of atoms geometrically do not interact with the ionization lasers due to the large opening angle of the effusion cone — they laterally travel out of the ionization volume defined by the laser beams in between laser pulses.

A Monte-Carlo type atom trajectory simulation is established and validated by comparison to theoretical descriptions. As a related observable directly accessible in the experimental environment of the PI-LIST, the atom density evolution along its central axis was probed for various tubular atom source geometries with a dedicated setup at the RISIKO mass separator at Mainz University. The results show the expected advantage of narrower atom source tubes and thus the applicability of the model. Pathways for further improvements are suggested.

2. PI-LIST ion source: Current status and optimization considerations

The Perpendicularly Illuminated Laser Ion Source and Trap PI-LIST as employed at ISOLDE is described in [3], the Mainz-type off-line version in [6], and first investigations of the atom density in this arrangement in [9,10]. Fig. 1 shows a 3-D model of the unit at ISOLDE. The unit is installed directly downstream of the standard ISOLDE hot cavity ion source, a tube with an inner diameter of 3 mm and length of 34 mm, before the extraction electrode to accelerate ions into the mass separator.

While the performance in terms of reducing the residual Doppler width of the experimentally obtainable laser spectroscopy spectra from typically several GHz down to a few 100 MHz is met, a limiting factor for many experiments is the significantly reduced efficiency of up to a factor of multiple 1000 compared to the standard RILIS in-source technique [3].

2.1. Efficiency optimization considerations

A main factor of the efficiency loss, both for standard collinear laser LIST operation as well as the perpendicular high-resolution mode, is the geometrical loss of the atoms effusing from the hot cavity out of the laser interaction region. As schematically indicated in Fig. 1 and investigated with various techniques in [9], the effusion resembles a wide cone rather than a well-collimated beam. As a result, the atom density along the central axis decreases proportionally to the inverse quadratic of the distance to the hot cavity. Fig. 2, adapted from [10], shows this effect for a previous version of the LIST at Johannes Gutenberg University Mainz. In the top graph, the potential along the beam axis is given inside the LIST structure, governed by the repeller electrodes. It indicates that in this geometry, ion extraction starts about 8 mm behind the cavity exit, at the point of the ridge of the electric potential. The bottom graph shows the strong decrease of ions experienced along the following 30 mm of path length that is available via transversal laser access (red line).

Optimizing the shape of the atomizing tube's effusion cone to direct more atoms along the central axis can significantly improve the efficiency of the PI-LIST technique. According to kinetic gas theory in low pressure regimes (no particle–particle interactions), the emission characteristics are solely determined by the ratio of the diameter and the length of the hot cavity tube [11]. By diverting from the standard geometry of the ISOLDE hot cavity towards a lower ratio of diameter to length, a more directed atom beam is expected to be produced. For standard collinear laser LIST operation, where the central volume is completely illuminated by the ionization lasers, this would bring a direct benefit without further adaptions. For PI-LIST operation, a geometry to cover a wider range of the volume with the perpendicular laser needs to be established, e.g. by introducing a multi-reflection path with multiple mirrors.

Employing thinner tube geometries is investigated systematically in this work. A simulation model using kinetic gas theory for atom effusion is developed and referenced to experimentally obtained results with different hot cavity geometries. The position-dependent relative atom density along the LIST central axis is used as an experimentally available observable of the atom beam collimation.

3. Atom effusion simulation model

The effusion of atoms from a hot cavity cylindrical oven was simulated in Wolfram Mathematica 13 with a Monte Carlo method in three-dimensional space. Individual atoms were randomly distributed at the back-end of the cylinder, which was treated as closed by a flat surface. This effectively replaces every atom leaving towards the back with another one coming in, thus resembles an infinite reservoir of constant atom density. Initial velocities were chosen from a

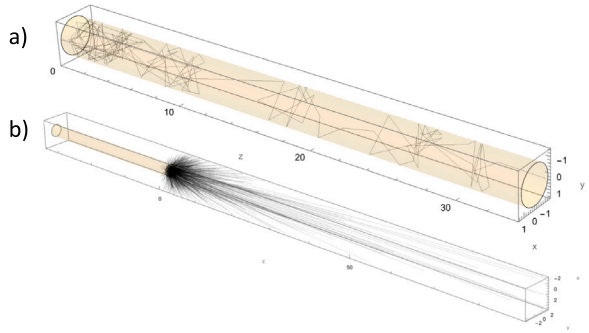

Fig. 3. Visualization of particle trajectories for the standard RISIKO atomizer cavity geometry ($D = 2.5$ mm, $L = 34$ mm). (a) Typical trajectory of a particle inside the cylinder. (b) 1000 trajectories of particles effusing out of the source. The shown z range of 90 mm behind the source corresponds to the length of an ISOLDE LIST unit.

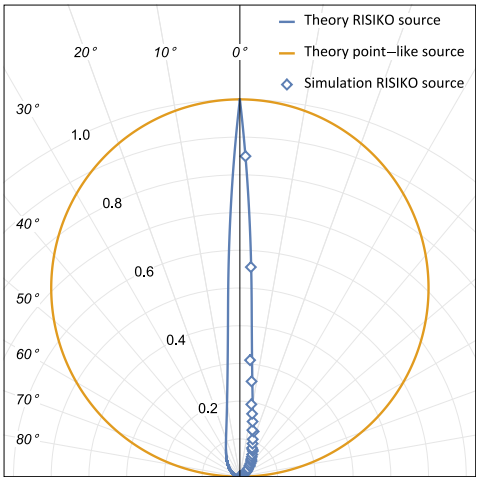

Fig. 4. Comparison of simulation results of lateral angle distribution to established theory for the standard RISIKO atom source, following the depiction of [11]: The semicircle grid lines indicate the relative ratio of particles being emitted under an angle denoted by the radial grid lines, with reference to perpendicular emission (ratio 1 at 0°). Theory results for a point-like atom source (Knudsen cosine law [12]) shown as reference.

Maxwell–Boltzmann distribution according to an adjustable temperature of the cylinder, and their direction from an isotropic distribution with forced positive component in axial direction. For the simulation of each individual trajectory, the following characteristics were implemented:

- **No particle–particle interaction.** The residual gas pressure in a target/ion source vacuum vessel is typically around 10^{-6} mbar, corresponding to a mean free path length of ≈ 100 m. Even if the local pressure in the atom source would be multiple orders of magnitude higher, the mean free path remains large compared to the ion source dimensions of a few millimeters.
- **The collision point with a wall is analytically calculated** from the equation of motion (starting point and velocity vector) and the border conditions of a given radius. Thus, no artifacts from coarse meshing can arise.
- **On collision with a wall, the particle is re-initialized at this position with a velocity according to the Maxwell–Boltzmann distribution and a direction according to the Knudsen cosine law** [12], i.e., the probability of emission under an angle θ to the surface normal scales with $\cos(\theta)$ — the emission direction is independent from the initial incidence. In physical terms, this corresponds to an adsorption, thermalization and re-emission of the particle on every wall contact.

At the point of exit from the cylinder, particle positions and velocities are recorded for statistical evaluation. The absolute values of velocity and thus the active travel times of the particles depend on the Maxwell–Boltzmann distribution (temperature and mass). However, the geometry of their trajectories does not. Spatial and angular characteristics of the ensemble are universally valid for effusion studies.

For visualization, Fig. 3 shows a typical trajectory of a single particle inside the cylinder (upper panel), and 1000 trajectories of effusing particles from the exit orifice (lower panel). The geometry corresponds to the standard hot atomizer cavity of the RISIKO mass separator with an inner diameter $D = 2.5$ mm and a length $L = 34$ mm. It is evident that the vast majority of the atoms leave under a considerable angle and are not available for laser ionization downstream on the central axis.

In order to validate the simulation results, the effusing atom characteristics were compared to established theoretical descriptions of low-pressure regime flow through tubular geometries [11–14]. An analogue approach was used, e.g., in [15], yet not with the scope of investigating the outgoing atom trajectories but studying the behavior inside the system. The characteristic statistic is the distribution of the velocity vector lateral angle θ in respect to the surface normal of the orifice area. The results are shown for the RISIKO-type atomizer cavity with the standard Knudsen law as reference in Fig. 4. The agreement between our simulations, given as diamonds on the positive quadrant side, and theory over the complete range strongly supports the adequateness of the simulation model.

The groundwork on molecular flow characteristics through tubes described above was later followed up upon in various ways. An analytical expression for the full width at half maximum (FWHM) angle $\theta_{1/2}$, defined by the angle at which the flow is half of the value compared to the flow at 0° is derived as $\theta_{1/2} = 1.68\, D/L$ in the molecular flow regime [16,17]. Fig. 4 also shows the adequateness of this expression at the example of the standard source: The blue graph intersects the half-circle denoting 0.5 under an angle of approximately 3.5°, being half of the calculated FWHM $\theta_{1/2} = 7.1°$.

In an additional cross-check, the time-averaged atom positions in the tube itself were investigated. The distribution exhibits an expected linear decrease in density from the back end of the tube (representing an infinite atom reservoir) up to the exit (negligible remaining partial pressure of species of interest) as commonly hypothesized in the context of atomic flux calculations for thin tubes (length ≫ diameter) [18].

To quantify the atom density available in the active volume of LIST-type ion sources, the diameters of the collinear laser beams have to be taken into account. In the simulations, a radius-adjustable cylindrical "ionization channel" around the central axis was implemented. The simulation records at which point this channel directly adjacent the hot cavity is penetrated by the atom trajectories. The respective travel distance within is added to the statistical evaluation. Note that for a laser diameter smaller than the hot cavity, atoms might not interact at all, or might be coming initially from outside the laser channel. As in reality the laser beam intensity is not uniform along its cross section but typically Gaussian, the results for different diameters can be used to estimate the relative contributions.

Simulations were conducted for three different geometries of hot cavities that were available for experimental investigations at the RISIKO mass separator. The respective dimensions with inner tube diameter D and tube length L are:

(A) RISIKO source: $D = 2.5$ mm, $L = 34$ mm ($\theta_{1/2} = 7.1°$)

(B) Multi-capillary source: 7 smaller tubes of $D = 0.5$ mm, $L = 30$ mm ($\theta_{1/2} = 1.6°$), arranged within a standard RISIKO source

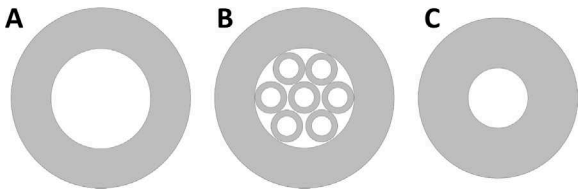

Fig. 5. To-scale visualization of investigated tube geometries. A: RISIKO standard source ($D = 2.5$ mm, $L = 34$ mm); B: Multi-capillary source (7 small tubes with $D_i = 0.5$ mm, $D_o = 0.8$ mm, $L = 30$ mm inside standard source); C: Thin source ($D = 1.5$ mm, $L = 34$ mm).

(C) Thin source: $D = 1.5$ mm, $L = 34$ mm ($\theta_{1/2} = 4.2°$)

The cross sections of the geometries are also visualized to-scale in Fig. 5.

The influence of the collinear laser's radial width, and potential angle or offset misalignment between hot cavity and laser beams, were also investigated systematically in the model. The observed deviations were determined to be minor and do not change the results and interpretations presented in this work.

4. Experimental setup

4.1. The RISIKO mass separator and laser system

The experimental part of this work was conducted at the RISIKO mass separator at the Institute of Physics at Johannes Gutenberg University Mainz. A detailed description of its current layout including a schematic overview is given in [19]. It features an ISOLDE-like front-end and ion source section and can thus serve as an ideal ion source development platform. The ions are extracted from the source at an electrical potential of 30 keV in two stages, shaped by an Einzel lens and subsequent deflector sets and a quadrupole triplet, and mass-over-charge-separated in a 60° dipole magnet with a subsequent slit diaphragm in its focal plane. The resulting mono-isobaric beam is re-focused onto either a Faraday Cup, or a secondary electron multiplier for single ion detection. For this work, the latter detection was employed in combination with a multichannel analyzer card (FAST ComTec MCA-3) to record individual ion arrival times in respect to the ionizing laser pulse.

The employed laser system consisted of two types of pulsed, wavelength-tunable titanium-doped sapphire (Ti:sa) lasers, a birefringent filter-tuned version [20] and a diffraction grating-based model [21]. The fundamental wavelength output range can be augmented by higher harmonic generation. The system is pumped by commercial frequency-doubled Nd:YAG lasers (Photonics Industries DM100-532) at a repetition rate of 10 kHz. The Ti:sa pulse duration is around 50 ns.

Manganese (Mn) was chosen as test element. The laser scheme employed for resonance ionization was the 3-step resonance scheme developed in [22]: a valence electron is promoted from the $3d^5 4s^2\ S_{5/2}$ ground state via the $3d^5 4s4p\ P^o_{7/2}$ (24802.25 cm^{-1}) and $3d^5 4s4d\ D_{7/2}$ (47212.06 cm^{-1}) excited states into an auto-ionizing state at 60939.09 cm^{-1}, utilizing laser vacuum wavelengths of 403.2 nm, 446.2 nm, and 728.5 nm, respectively. While the first and second step were shown to be saturated with the available power levels of 260 mW and 100 mW, the ionizing transition was not saturated at 400 mW [22].

4.2. The PI-LIST ion source with external laser access

The infrastructure for the investigations presented here was the Mainz version of the PI-LIST, schematically shown in Fig. 6. In contrast to the ISOLDE version, it features lateral laser access by a 30 mm diameter entrance window at the side of the ion source vacuum vessel.

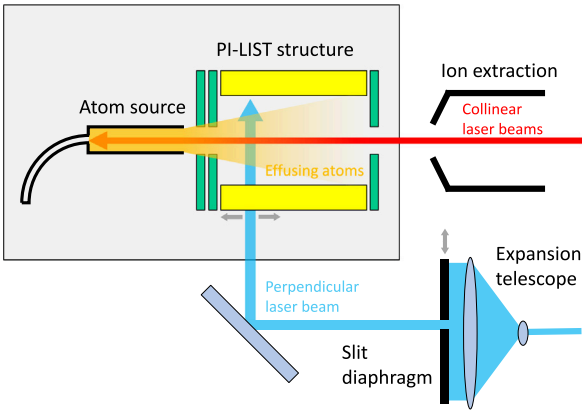

Fig. 6. Schematic of the technique for screening the atom density along the LIST central axis. Moving a slit diaphragm in a horizontally widened laser beam translates to changing the overlap volume of all lasers, i.e. the sole point of ionization.
Source: Figure adapted from [9].

This allows for translation of the perpendicular laser along the central axis of the LIST unit to probe the ion production rate at various locations. The technique and setup are described in detail in [9]. The perpendicular laser beam (first excitation step) is expanded along the LIST central axis with a cylindrical lens telescope. A slit diaphragm allows then the selection of a part of it, corresponding to ionization only in the respective overlap spot with the collinear laser beams inside the LIST. It was verified that the expansion factor of the beam is high enough so that the power of the portion transmitted through the slit is independent from the slit position. Assuming no position dependency of ionization efficiency, laser overlap and ion extraction, this technique allows for screening of the atom density in the laser overlap volume.

The Mn atoms were provided from a sample of commercial standard solution (Fisher Scientific AAS standard solution, Specpure Mn 1000 µg/mL). From a 1:1000 dilution with de-ionized water, 0.5 µL (corresponding to around $5 \cdot 10^{12}$ Mn atoms) were dried on a zirconium foil. The foil was folded and inserted into the independently heatable reservoir capillary directly connected to the back of the atom source.

4.3. Investigated atom sources

Three different atom source geometries were constructed from tantalum to be tested in comparison, corresponding to the simulation models described in Fig. 5. The standard RISIKO source (for more details see [23]) and the thin source were machined in the mechanical workshop of the Institute of Physics at Mainz University. The multi-capillary source was constructed by cutting a commercially available long tantalum capillary into 30 mm long sections and manually inserting them into a standard RISIKO source. During the process of installation at RISIKO, the capillaries shifted back inside the tube by 3 mm, which was taken into account in the data evaluation. A photograph of the assembly is shown in Fig. 7. The outer diameter of the thin source was chosen so that the cross section area of the wall is equal to the standard source. Thus, a comparable electrical resistivity and therefore similar temperature behavior for a given heating current is achieved. The atom sources are ohmically heated by applying a current of 250 A, corresponding to a temperature of around 1800 °C.

5. Experimental results and discussion

5.1. Absolute position calibration between experiment and simulation

A prerequisite for the comparative analysis is the calibration of the distance of the probing volume from the exit of the atom source for

Fig. 7. Photograph of the multi-capillary atom source, corresponding to model B in Fig. 5. The individual capillaries are placed inside a standard RISIKO source. The larger cylinder visible around serves as a heat screen during operation and is not an active part of the atom source.

each dataset. The axial position of the lateral laser beam could only be recorded on a relative scale at the point where the slit diaphragm was moved, behind the beam expansion telescope (see Fig. 6). The subsequent laser travel path was still approximately 1.5 m. Following the approach in [10], the individual ion arrival time structures for every setpoint of the perpendicular laser position were utilized for calibration: Depending on the ion starting positions, the observed ion arrival pattern of a thermal ion ensemble traveling through the LIST and the subsequent separator structure will be different — the individual features of this time structure are well-understood [5]. Ions created in the field of the repelling electrodes (see Fig. 8, upper graph) experience a push towards the exit and are thus extracted earlier than ions created in the center of the LIST, which travel according to their thermal distribution and also exhibit a broader time distribution. Ions created at the back of the LIST, directly in the penetrating extraction field, arrive at the detector earliest.

Trajectories of 20,000 ions were simulated in SIMION 8.2 [24], initialized with starting positions on the central axis of a LIST structure and with velocity components in positive z direction taken from a Maxwell–Boltzmann distribution. The simulation infrastructure includes the field generated by the LIST repeller electrodes, the RISIKO setup with two-stage extraction into the separator beam line on ground potential, the Einzel lens and subsequent field-free drift to the detector without change of ion velocity.

The starting-position-dependent simulated time structure can then be overlaid with the measured time structure for the different lateral laser positions taken during the experiment. The measurement data is normalized to the respective maximum of each single measurement slice for better visualization of the time structure. Adjustment of the position scale of the experimental data, combined with the uncertainty of the diaphragm slit setting, enables calibration of the actual position of the lateral laser beam in the LIST to 1 mm accuracy. Visualization of the data overlay for calibration of the standard ion source measurements is shown in Fig. 8, lower graph.

There is a distinct feature in the measured time structure pattern of ions apparently arriving around 28 µs for lateral laser positions of less than 5 or more than 32 mm distance from the hot cavity, that is not produced by the simulation. It is explained by the fact that at these settings, the lateral laser at least partially illuminates the edge of the 30 mm diameter entrance window. Diffusely reflected laser light then illuminates the whole volume inside the LIST. The time structure is then dominated by ions originating from the point of highest atom density, i.e., from the position directly behind the electric potential ridge at

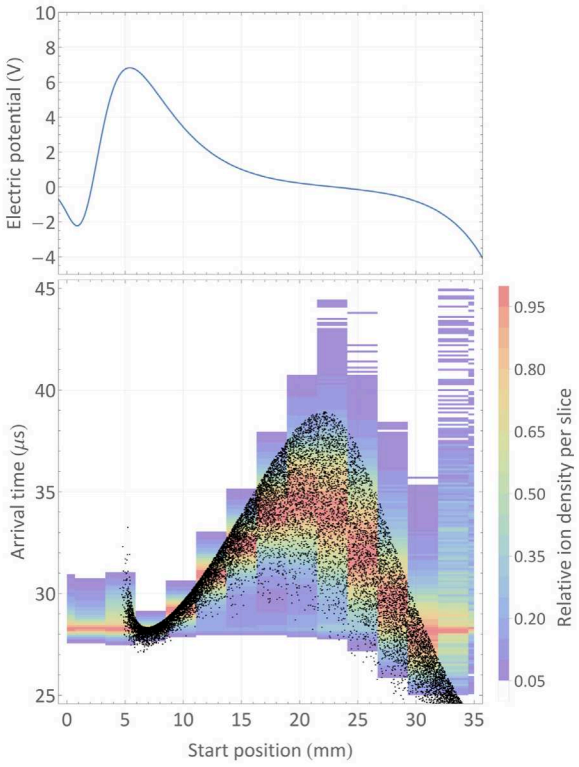

Fig. 8. Bottom: Visualization of measured (colored background - position calibration already applied) and simulated (black individual dots) ion arrival time structures in dependence of the ion starting positions. Top: Electric potential along the central axis with the applied LIST electrode settings (corresponding to the presentation in upper panel of Fig. 2). Correspondence between simulation and measurement confirms the adequateness of the chosen calibration between recorded diaphragm position and actual lateral laser position in the LIST corpus (see Fig. 6).

around 7–8 mm, where there is a perfect agreement of simulation and experimental data. Thus, the described feature in the measurement data can be disregarded as artifact.

5.2. Experimental data preparation

A full dataset recording for a chosen atom source geometry took around two hours. For the presented investigations, it is crucial to disentangle changes in ionization rate due to external factors (e.g., sample depletion) from the influence of the ionization position. For this reason, the slit diaphragm in the lateral laser beam was removed before, during and after the measurement, to monitor the overall ionization rate with full laser illumination of the central axis of the LIST. The individual data points were normalized using a linear interpolation of these references.

Additionally, the non-laser related background ion rate is accounted for. As for every data point the whole time structure between two laser pulses of 100 µs is recorded, a time gate can be set outside the arrival times of laser-ionized ions on the detector. As can be seen in Fig. 8, this is guaranteed for arrival times later than 50 µs. Here, only ions that are not created by the laser, but by other mechanisms such as remaining surface ionization or electron impact, are detected. The ion rate from this time gate is scaled to the complete time window and subtracted from the overall rate to yield the purely laser-ionized fraction.

While this data treatment provides an intrinsically normalized dataset for every ion source geometry, a comparison of the absolute ion rate between the measurement with different ion source geometries is not possible. The physical exchange of the source requires a full

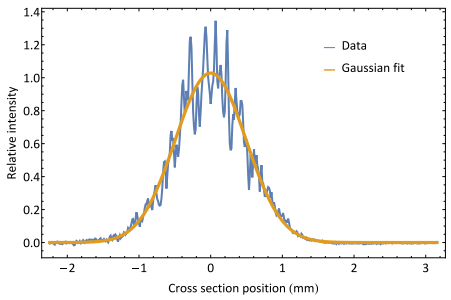

Fig. 9. Laser beam cross section profile of the ionization step. Based on this measurement, an ionization channel diameter of 2 mm, corresponding to the $1/e^2$ width, is used in the simulations.

cooling and heating cycle with manual assembly of the hot cavity and sample reservoir. A part of the sample might potentially condense in the removed source instead of re-used reservoir. Additionally, the atom source temperature might vary between different versions even though the ohmic heating power was kept constant, as different electric contact resistances or the geometries itself can play a role. A direct monitoring of the temperature was not possible in the experimental setup. These effects lead to possible changes in available Mn atom supply and its evaporation rate between the different measurements that cannot be quantified. Thus, every dataset is scaled to its respective maximum ionization rate, corresponding to ionization in the volume directly downstream of the electric potential ridge, where the atom density is the highest. The relative evolution of the atom density from this point onward serves as the experimental observable to compare the different source geometries and relate them to the simulation results.

5.3. Comparison of experiment and simulation results

As the ionization step laser did not provide sufficient power to saturate the transition, its spatial profile defines the cross section of the ionization cylinder inside the LIST. A beam profile cross section measurement (CinCam CMOS 1202) at this position is depicted in Fig. 9. Based on this measurement, an ionization channel cross section of 2 mm diameter, corresponding to the $1/e^2$ width, was chosen for the comparative simulations.

The results of the experimental campaign and the simulations are shown in comparison in Fig. 10. The simulation data was also scaled to its respective maximum at a distance of 7.5 mm from the atom source exit, i.e. the position of the electric potential ridge. For consistency, only the measurement data for which there are no restrictions to the ionization and transmission is shown, i.e., behind the potential ridge and before the lateral laser is partially blocked by the entrance window (see also Fig. 8). Error bars on the experimental values are derived from the position calibration (Section 5.1) on the horizontal axis, and a combination of Poisson statistics on absolute counts and the normalization to time-dependent signal changes (Section 5.2) on the vertical axis. For the simulation, the shaded error bands are based on Poisson statistics on the number of simulated particles (20,000 each for the standard and thin source, 6000 for the multi-capillary source).

Fig. 10 shows a general agreement between the experimental and simulation data trends. The relative decrease of the ion rate for the multi-capillary source is less pronounced than for the other two test geometries. Both the standard source and thin source are on a comparable level. However, systematic discrepancies occur between experimental data and simulation results. Especially for higher distances, the simulation overestimates the actual remaining ion rate in all cases. Generally, the experimentally measured relative ion rates seem to consistently be a factor 2 below the simulation results for source distances of greater than 10 mm. This deviation between experimental data and simulation values is not fully understood. It cannot be ascribed to an inferior spatial overlap of the collinear lasers over this distance: The laser beams converge from their launch points (where they are maximum of 1 cm apart) outside the separator magnet over approx. 4 m. At the start of each measurement run, the laser beams were spatially optimized in all-collinear mode for the highest ion rate, which would lead to the best overlap being in the highest atom density volume just behind the repelling potential ridge. The overlap displacement over the range inside the LIST thus geometrically is less than 0.05 mm. A possible reason for the discrepancy could be seen in a lower transmission efficiency of ions created further downstream in the LIST body. These ions do not profit from an initial acceleration by the repelling electric field towards extraction and might experience higher losses. Another possible effect is the different electric starting potential of the ions: As shown in the upper graph in Fig. 8, it can defer by up to 6 V between ions created directly behind the potential ridge and those more inwards. The energy spread acceptance of the RISIKO separator magnet is in the order of 10 V, and the nominal mass setting was optimized on the highest count rate coming from the high atom density at the slightly higher starting potential. Thus, the transmission of the lower-energy ions from the center of the LIST body can also be reduced.

Another difference is the ordering of the relative declines between thin and standard source, where the simulation predicts a slight advantage for the standard source up to around 30 mm. The experimental data does not show this advantage with statistical significance.

In conclusion, the agreement in the trends and especially the accordance in relative ion rate between the different geometries in both, experiment and simulation, fully supports the adequateness of the simulation model for further work.

5.4. Implications for LIST-type laser ion sources

In order to draw conclusion from the simulation model for an absolute instead of relative quantification, the available atom density in a 2 mm diameter cylindrical volume around the central axis behind the respective atom source is depicted in Fig. 11. The vertical axis shows the remaining fraction of all atoms in the simulation, opposed to being scaled to a certain position as in Fig. 10.

This result shows an advantage of the non-standard geometries, i.e. multi-capillary and thin, over the 2.5 mm diameter standard RISIKO type source. An average of 30% atom density enhancement in the ionization channel can be achieved with both new geometries in the entire examined range. The difference between the thin source and the multi-capillary source is marginal. This is due to the arrangement of multiple capillaries in the cluster of 7 and thus still yielding a comparable cross section area for the atom effusion, while using a single capillary as sole source would bring another significant advantage of almost a factor 2 enhancement compared to the standard source.

A central outcome of this study, as already also discussed in [5,9], is the significance of close proximity of the active ionization region to the atom source exit. This holds true for all atom source geometries. Designing both mechanical parts and shaping the electric potential in a way to extract ions from as close as possible to the source exit would yield the highest geometric efficiency increase.

For the high resolution laser spectroscopy in perpendicular illumination mode, another aspect has to be taken into account. Due to the geometry of the diverging cone of the effusing atoms, the distribution of the lateral velocity classes of the atoms in the ionization channel will be broader when closer to the atom source. The specific influence of the atom source geometry on this effect is subject to upcoming investigations using the developed simulation model and narrow-bandwidth laser infrastructure.

From operational point of view, especially at on-line facilities such as ISOLDE, the atomizer geometry also plays a vital role in atom retainment. Thinner tubes lead to a significant increase in the average number of wall collisions of atoms traveling through. This number

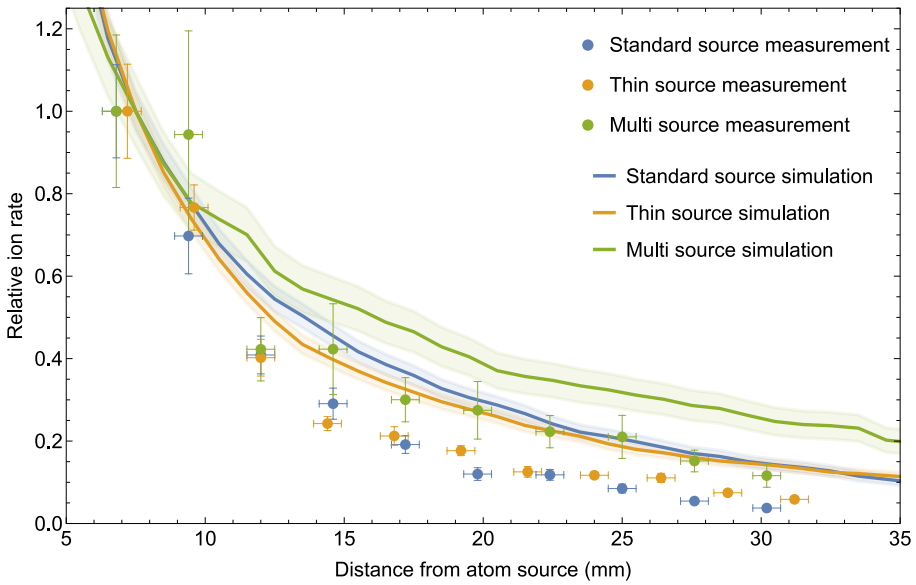

Fig. 10. Comparison of experimental results and simulation values for relative ion rate in respect to distance from atom source, normalized to ion rate at 7.5 mm distance. Error bars are calculated as $\sqrt{N}$ for the number N of detected particles on the detector in the experiment, or simulated particles in the Monte Carlo model. See text for discussion.

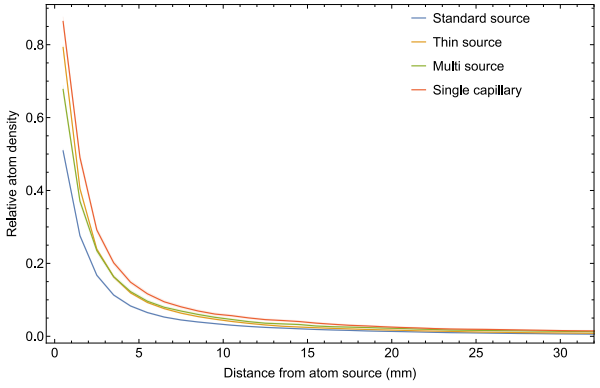

Fig. 11. Comparison of simulation results for atom density within active laser ionization volume around central axis for the different ion source geometries.

can be estimated from the ratio of the area of the exit to the overall wall area [25]. By changing from the RISIKO standard source to a single capillary, the number of collisions would increase by a factor of around 5. Especially for short-lived species, or long wall adhesion times, this can become a significant influence. Additionally, the overall surface ionization efficiency rises accordingly, increasing losses of the element of choice by blocking it from entering the LIST structure by getting ionized already in the hot cavity, before the repeller electrodes. Lastly, long-term material integrity tests to investigate possible clogging or mechanical deformation effects must be conducted before implementation.

6. Conclusion and outlook

A Monte–Carlo-type simulation model to describe the effusion of atoms from hot cavity tubes of various dimensions has been developed for application in LIST-type laser ion sources. The simulated ensemble data is validated by comparison with theoretical descriptions of low-pressure particle transfer mechanisms. The evolution of the atom density along the central axis directly downstream from the hot cavity, presenting a relevant observable of LIST-type ion sources, was experimentally determined for different geometries. The use of a standard PI-LIST unit for these experiments ensures transferability of the results. As expected, slimmer tubes produce a more directed atom stream, resulting in a less pronounced relative decline of density moving away from the cavity orifice. Correspondingly, higher overall ionization efficiency is expected due to a higher available atom fraction in the laser interaction volume downstream and less radial geometric losses of atoms — a relative increase of 30% is derived for the investigated models. While this work focuses on analysis of the atom density in comparison to experimental data, the developed simulation infrastructure has a broader scope and is intended to be used for further studies of atom behavior in (laser) ion sources, e.g., regarding remaining Doppler broadening in perpendicular laser geometry as in PI-LIST, e.g. following up on the work in [26], or atom retainment inside the hot cavity. More complex atom source geometries can be explored computationally before physical prototyping.

Complimentary methods of characterization of the atom effusion could entail density measurements by planar laser-induced fluorescence (PLIF) [27]. Additionally, spatial distribution of material depositions on catcher foils placed at varying distances to a hot cavity could be investigated with ellipsometry [28].

CRediT authorship contribution statement

Asar A.H. Jaradat: Writing – original draft, Visualization, Validation, Software, Resources, Project administration, Methodology, Investigation, Formal analysis, Data curation, Conceptualization. **Reinhard Heinke:** Writing – review & editing, Visualization, Validation, Supervision, Software, Resources, Project administration, Methodology, Investigation. **Bruce A. Marsh:** Funding acquisition, Conceptualization. **Dominik Studer:** Resources, Investigation. **Kara M. Lynch:** Writing – review & editing, Supervision, Funding acquisition. **Kieran T. Flanagan:** Supervision, Funding acquisition. **Klaus Wendt:** Writing – review & editing, Supervision, Funding acquisition. **Matou Stemmler:** Resources. **Sebastian Raeder:** Resources. **Sebastian Rothe:** Supervision. **Simone Gilardoni:** Supervision. **Thorben Niemeyer:** Resources. **Raphael Hasse:** Resources.

Declaration of competing interest

The authors declare that they have no known competing financial interests or personal relationships that could have appeared to influence the work reported in this paper.

Acknowledgments

This work has received funding from the European Union's Horizon 2020 Research and Innovation Programme under grant agreement project number 861198 (LISA) Marie Sklodowska-Curie Innovative Training Network (ITN). K.M.L. and R.H. acknowledge support from UK Research and Innovation (UKRI) under the UK government's Horizon Europe funding guarantee grant EP/Y036816/1 (ESPEN). K.M.L. acknowledges support from the Royal Society Dorothy Hodgkin Fellowship grant DHf\RI\231007. This work has been supported by the Bundesministerium für Bildung und Forschung (BMBF, Germany) under project 05P21UMFN3. We thank the mechanical workshop of the Institute of Physics of Johannes Gutenberg University for excellent manufacturing of the PI-LIST and atom source components.

Data availability

Data will be made available on request.

References

[1] V. Fedosseev, K. Chrysalidis, T.D. Goodacre, B. Marsh, S. Rothe, C. Seiffert, K. Wendt, Ion beam production and study of radioactive isotopes with the laser ion source at ISOLDE, J. Phys. G: Nucl. Part. Phys. 44 (8) (2017) 084006, http://dx.doi.org/10.1088/1361-6471/aa78e0.

[2] X.F. Yang, S.J. Wang, S.G. Wilkins, R.G.F. Ruiz, Laser spectroscopy for the study of exotic nuclei, Prog. Part. Nucl. Phys. 129 (2023) 104005, http://dx.doi.org/10.1016/j.ppnp.2022.104005.

[3] R. Heinke, M. Au, C. Bernerd, K. Chrysalidis, T.E. Cocolios, V.N. Fedosseev, I. Hendriks, A.A.H. Jaradat, M. Kaja, T. Kieck, et al., First on-line application of the high-resolution spectroscopy laser ion source PI-LIST at ISOLDE, Nucl. Instruments Methods Phys. Res. Sect. B: Beam Interactions Mater. Atoms 541 (2023) 8–12, http://dx.doi.org/10.1016/j.nimb.2023.04.057.

[4] D.A. Fink, S.D. Richter, B. Bastin, K. Blaum, R. Catherall, T.E. Cocolios, D.V. Fedorov, V.N. Fedosseev, K.T. Flanagan, L. Ghys, et al., First application of the laser ion source and trap (LIST) for on-line experiments at ISOLDE, Nucl. Instruments Methods Phys. Res. Sect. B: Beam Interactions Mater. Atoms 317 (2013) 417–421, http://dx.doi.org/10.1016/j.nimb.2013.06.039.

[5] D.A. Fink, T.E. Cocolios, A.N. Andreyev, S. Antalic, A.E. Barzakh, B. Bastin, D.V. Fedorov, V.N. Fedosseev, K.T. Flanagan, L. Ghys, et al., In-source laser spectroscopy with the laser ion source and trap: First direct study of the ground-state properties of ^{217,219}Po, Phys. Rev. X 5 (1) (2015) http://dx.doi.org/10.1103/physrevx.5.011018.

[6] R. Heinke, T. Kron, S. Raeder, T. Reich, P. Schönberg, M. Trümper, C. Weichhold, K. Wendt, High-resolution in-source laser spectroscopy in perpendicular geometry, Hyperfine Interact. 238 (1) (2016) http://dx.doi.org/10.1007/s10751-016-1386-2.

[7] D. Studer, J. Ulrich, S. Braccini, T.S. Carzaniga, R. Dressler, K. Eberhardt, R. Heinke, U. Köster, S. Raeder, K. Wendt, High-resolution laser resonance ionization spectroscopy of $^{143-147}$Pm, Eur. Phys. J. A 56 (2) (2020) http://dx.doi.org/10.1140/epja/s10050-020-00061-8.

[8] T. Kron, R. Beerwerth, S. Raeder, S. Fritzsche, R. Heinke, P. Schönberg, M. Trümper, K. Wendt, Hyperfine structure study of ^{97,98,99}Tc in a new laser ion source for high-resolution spectroscopy, Phys. Rev. C 102 (3) (2020) http://dx.doi.org/10.1103/physrevc.102.034307.

[9] R. Heinke, V. Fedosseev, T. Kieck, T. Kron, B. Marsh, S. Raeder, S. Richter, S. Rothe, K. Wendt, Atom beam emersion from hot cavity laser ion sources, Nucl. Instruments Methods Phys. Res. Sect. B: Beam Interactions Mater. Atoms 463 (2020) 449–454, http://dx.doi.org/10.1016/j.nimb.2019.04.026.

[10] R.M. Heinke, In-Source High-Resolution Spectroscopy of Holmium Radioisotopes - on-Line Tailored Perpendicular Laser Interaction At ISOLDE'S Laser Ion Source and Trap LIST (Ph.D. thesis), Johannes Gutenberg-Universität Mainz, 2019, http://dx.doi.org/10.25358/openscience-2346.

[11] P. Clausing, Über die strahlformung bei der molekularströmung, Z. Phys. 66 (7–8) (1930) 471–476, http://dx.doi.org/10.1007/BF01402029.

[12] M. Knudsen, Die gesetze der molekularströmung und der inneren reibungsströmung der gase durch röhren, Ann. Phys., Lpz. 333 (1) (1909) 75–130, http://dx.doi.org/10.1002/andp.19093330106.

[13] M. Knudsen, Die molekularströmung der gase durch öffnungen und die effusion, Ann. Phys., Lpz. 333 (5) (1909) 999–1016, http://dx.doi.org/10.1002/andp.19093330505.

[14] H. Mayer, Über eine experimentelle methode zur messung von molekularstrahlung, Z. Phys. 52 (3–4) (1929) 235–248, http://dx.doi.org/10.1007/BF01342399.

[15] Y. Liu, M. Smith, Computational Studies of Solid Stoppers for Generating Intense Exotic Radioactive Ion Beams at FRIB, Tech. Rep., Oak Ridge National Laboratory (ORNL), Oak Ridge, TN (United States), 2018, http://dx.doi.org/10.2172/1484136.

[16] J.A. Giordmaine, T.C. Wang, Molecular beam formation by long parallel tubes, J. Appl. Phys. 31 (1960) 463–471, http://dx.doi.org/10.1063/1.1735609.

[17] F. Rugamas, D. Roundy, G. Mikaelian, G. Vitug, M. Rudner, J. Shih, D. Smith, J. Segura, M.A. Khakoo, Angular profiles of molecular beams from effusive tube sources: I. experiment, Meas. Sci. Technol. 11 (2000) 1750–1765, http://dx.doi.org/10.1088/0957-0233/11/12/315.

[18] V.N. Fedoseyev, G. Huber, U. Köster, J. Lettry, V.I. Mishin, H. Ravn, V. Sebastian, The ISOLDE laser ion source for exotic nuclei, Hyperfine Interact. 127 (2000) 409–416, http://dx.doi.org/10.1023/A:1012609515865.

[19] T. Kieck, H. Dorrer, C.E. Düllmann, V. Gadelshin, F. Schneider, K. Wendt, Highly efficient isotope separation and ion implantation of ^{163}Ho for the ECHo project, Nucl. Instruments Methods Phys. Res. Sect. A: Accel. Spectrometers, Detect. Assoc. Equip. 945 (2019) 162602, http://dx.doi.org/10.1016/j.nima.2019.162602, URL https://www.sciencedirect.com/science/article/pii/S016890021931109X.

[20] C. Mattolat, S. Rothe, F. Schwellnus, T. Gottwald, S. Raeder, K. Wendt, T. Iguchi, K. Watanabe, An all-solid-state high repetiton rate titanium:Sapphire laser system for resonance ionization laser ion sources, in: AIP Conference Proceedings 1104, AIP, 2009, pp. 114–119, http://dx.doi.org/10.1063/1.3115586.

[21] A. Teigelhöfer, P. Bricault, O. Chachkova, M. Gillner, J. Lassen, J.P. Lavoie, R. Li, J. Meißner, W. Neu, K.D.A. Wendt, Grating tuned Ti:sa laser for in-source spectroscopy of Rydberg and autoionizing states, Hyperfine Interact. 196 (2010) 161–168, http://dx.doi.org/10.1007/s10751-010-0171-x.

[22] Separation of manganese isotopes by resonance ionization mass spectrometry for ^{53}Mn half-life determination, Eur. Phys. J. Appl. Phys. 97 (2022) 19, http://dx.doi.org/10.1051/epjap/2022210270.

[23] T. Kieck, S. Biebricher, C.E. Düllmann, K. Wendt, Optimization of a laser ion source for ^{163}Ho isotope separation, Rev. Sci. Instrum. 90 (2019) http://dx.doi.org/10.1063/1.5081094.

[24] D. Manura, D. Dahl, SIMION 8.1 User Manual, Rev-5, Adaptas Solutions, LLC, Palmer, MA, 2008.

[25] R. Kirchner, Progress in ion source development for on-line separators, Nucl. Instrum. Methods Phys. Res. 186 (1981) 275–293, http://dx.doi.org/10.1016/0029-554X(81)90916-2.

[26] E. Granados, G. Stoikos, C. Bernerd, K. Chrysalidis, D.T. Echarri, V.N. Fedosseev, R. Heinke, B.A. Marsh, In-source high-resolution spectroscopy using an integrated tunable Raman laser, Laser Photonics Rev. 18 (2024) http://dx.doi.org/10.1002/lpor.202300564.

[27] A. Zadvornaya, P. Creemers, K. Dockx, R. Ferrer, L.P. Gaffney, W. Gins, C. Granados, M. Huyse, Y. Kudryavtsev, M. Laatiaoui, E. Mogilevskiy, S. Raeder, S. Sels, P. van den Bergh, P. van Duppen, M. Verlinde, E. Verstraelen, M. Nabuurs, D. Reynaerts, P. Papadakis, Characterization of supersonic gas jets for high-resolution laser ionization spectroscopy of heavy elements, Phys. Rev. X 8 (4) (2018) http://dx.doi.org/10.1103/PhysRevX.8.041008.

[28] R.M.A. Azzam, N.M. Bashara, Ellipsometry and Polarized Light, North-Holland, Elsevier, Amsterdam and Lausanne and New York, 1996.